When Van Gogh meets Mandelbrot: Multifractal classification of painting's texture

Patrice Abry, Herwig Wendt, Stéphane Jaffard

When Van Gogh meets Mandelbrot: Multifractal classification of painting's texture

P. Abry [a,*], H. Wendt [b], S. Jaffard [c]

[a] Physics Department, ENS Lyon, CNRS, Lyon, France
[b] IRIT - ENSEEIHT, Toulouse Univ., CNRS, Toulouse, France
[c] Math. Dept., Paris Est Univ., Créteil, France

A B S T R A C T

Recently, a growing interest has emerged for examining the potential of Image Processing tools to assist Art Investigation. Simultaneously, several research works showed the interest of using *multifractal analysis* for the description of homogeneous textures in images. In this context, the goal of the present contribution is to study the benefits of using the wavelet leader based multifractal formalism to characterize paintings. After a brief review of the underlying key theoretical concepts, methods and tools, two sets of digitized paintings are analyzed. The first one, the *Princeton Experiment*, consists of a set of seven paintings and their replicas, made by the same artist. It enables examination of the potential of multifractal analysis in forgery detection. The second one is composed of paintings by Van Gogh and contemporaries, made available by the Van Gogh and Kröller-Müller Museums (Netherlands) in the framework of the *Image processing for Art Investigation* research program. It enables us to show various differences in the regularity of textures of Van Gogh's paintings from different periods, or between Van Gogh's and contemporaries' paintings. These preliminary results plead for the constitution of interdisciplinary research teams consisting of experts in art, image processing, mathematics and computer sciences.

1. Introduction

1.1. Image processing for art investigation

The ever growing power of digital devices (faster processors, better computers, higher resolution scanners, larger storage facilities, etc.) naturally and unavoidably gave birth to the desire of using such tools for Art Investigation. Yet, it is only recently, at the turn of the 3rd millennium, that conditions were met to transform this desire into some form of reality. Various research groups started to apply standard image processing tools to digitized painting, to develop new procedures, or to customize existing ones to meet the specificities of such an application (cf. [19] for an example of early contribution, [17,20] for review notes, and [12,21,22,8] for presentations of state-of-the-art and/or joint recent research contributions). With the development of computer-assisted and statistical signal-image processing tools, it is not the aim of scientists to supplant art historians, but rather to provide them with additional attributes that can be extracted automatically using objective and reproducible criteria. This will allow progress by diversification of the tools at hand. For paintings, it may for instance help to assess quantitative measures related to stylometry, brushstrokes, texture, etc. (cf. e.g., [24,13], where digital texture and brushstroke features are used to characterize paintings of Van Gogh). This may contribute to the formulation of answers to questions, such as what period was a painting created, is a painting authentic or a forgery, and has it been correctly attributed to an artist.

* Corresponding author.
E-mail address: patrice.abry@ens-lyon.fr (P. Abry).
URL: http://perso.ens-lyon.fr/patrice.abry (P. Abry).

1.2. Wavelet and fractal for image processing

Over the last 15 years, elaborating on multiresolution decomposition and filter banks, wavelet analysis has become one of the inescapable image processing tools. In essence, wavelet coefficients evaluate the content of an image at a given space position $\mathbf{x}=(x_1,x_2)$ and a given analysis scale a. Wavelet coefficients usually take large values when the corresponding wavelet is located on any of the contours of the image, while they fluctuate around small values when the wavelet is located inside smooth textures. For an introduction, review and examples, the reader is referred to e.g., [14]. The statistical properties of wavelet coefficients have already been successfully used in stylistic analysis of paintings and forgery detection, cf. e.g., [9,12,15].

Fractal geometry refers to an analysis paradigm that relies on the idea that the richest part of the information to be extracted from an image lies in the way the statistics of some space-scale dependent quantities vary as a function of the analysis scale a. In other words, instead of basing the analysis on the search of specific features of space-scales, it is preferred to postulate that all space-scales are jointly and equally important and that the key information lies in the mechanisms relating them to each other. This dependence is usually postulated in the form of power laws: a^{ζ} (with ζ referred to as the *scaling exponent*) which explains why *fractal* is also termed *scaling* or *scale invariance*. Wavelet analysis consists in decomposing an image on elementary shapes (the wavelet basis) which are all deduced from three fundamental functions, the *mother wavelets*, by translation and dilation, see Eq. (1). Scaling invariance properties of the image will imply power-law behaviors of the wavelet coefficients. Therefore, in essence, wavelets constitute a *natural* decomposition system for characterizing fractal properties of images. Fractal tools can be used both for the analysis of contours and textures. There is a rich literature discussing the relevance of fractal paradigms to analyze or model natural images, a recent and interesting review can be consulted in [4]. In the context of Art, it was used in [18] to characterize some of Jackson Pollock's masterpieces.

1.3. Goals, contributions and outline

Beyond *fractal* analysis, essentially aiming at characterizing how *irregular* an object is globally by means of a single scaling exponent, *multifractal* analysis consists of a signal/image processing tool that concentrates on describing the fluctuations along space of the local regularity of the object, which requires the use of whole collections of scaling exponents. While popular for the analysis of 1D signals, multifractal analysis remained rarely used in image processing applications for both theoretical and practical reasons (cf. a contrario [2]). However, this situation has recently been changed when it was shown that a theoretically sound and practically efficient formulation of multifractal analysis could be obtained on the basis of wavelet leaders, a simple construction elaborating on 2D discrete wavelet transform coefficients, cf. [10,11,28,30,1]. This wavelet leader multifractal analysis constitutes a powerful tool for the analysis of textures in images, as detailed theoretically in [30] and explored practically in [29].

The present contribution aims at exploring the potential of the wavelet leader multifractal analysis for art painting texture classification. First (cf. Section 2), the principles and practical procedures underlying the wavelet leader multifractal analysis will be presented in a manner geared towards practitioners (hence avoiding theoretical developments and proofs, for which the reader will be referred to earlier publications). These procedures will be illustrated on several paintings. Then (cf. Section 3), it will be shown when and how the wavelet leader multifractal analysis enables to discriminate between original paintings and replicas. This will be embedded in the context of an original experiment conducted by the *Machine Learning and Image Processing for Art Investigation Research Group* at Princeton University (cf. www.math.princeton.edu/ipai/index.html). Finally (cf. Section 4), the wavelet leader multifractal analysis will be applied to a set of Van Gogh's and contemporaries' paintings, made available by the Van Gogh and Kröller-Müller Museums (The Netherlands) within the *Image Processing for Art Investigation* research project (cf. www.digitalpaintinganalysis.org/).

2. Multifractal analysis

2.1. Wavelet coefficients and global regularity

2.1.1. 2D discrete wavelet transform

An orthonormal wavelet basis in two dimensions is constructed from three smooth, compactly supported functions $\psi^{(1)},\psi^{(2)},\psi^{(3)}$, which are chosen such that the system

$$\psi^{(m)}_{j,(k_1,k_2)}(x_1,x_2)=2^{-j}\psi^{(m)}(2^{-j}x_1-k_1,2^{-j}x_2-k_2),\quad j,k_1,k_2\in\mathbb{Z},\ m=1,2,3 \tag{1}$$

constitutes an orthonormal basis of $L^2(\mathbb{R}^2)$. This system is called a wavelet basis, and the three functions $\psi^{(1)},\psi^{(2)},\psi^{(3)}$ its mother wavelets. Let $X(\mathbf{x})$ (with $\mathbf{x}=(x_1,x_2)$) denote a gray level image. We denote by $D_X^{(m)}(j,\mathbf{k})$ (with $\mathbf{k}=(k_1,k_2)$, $m=1, 2, 3$) the coefficients of the image X on this wavelet basis, which are given by the inner product with the basis functions, $D_X^{(m)}(j,\mathbf{k})=\langle X|\psi^i_{j,k}\rangle$. Note that in practice these wavelet coefficients are not computed as integrals, but using the classical pyramidal recursive algorithm supplied by the *fast wavelet transform*. Qualitatively, the coefficient $D_X^{(m)}(j,\mathbf{k})$ measures the amount of energy of the image X that is contained, in the spatial neighborhood of width $\sim 2^j$ located at position $(2^jk_1,2^jk_2)$, in the frequency bands localized around $\pm 2^{-j}$. For an introduction to the 2D discrete wavelet transform (2D DWT), the reader is referred to e.g., [14].

In the present contribution, it has been chosen to work with mother wavelets obtained as tensor products of the minimal compact support Daubechies wavelet families, which are parametrized by their number of vanishing moments N_ψ [5]. It has been discussed elsewhere that this family has ideal theoretical and practical properties with respect to scaling and fractal analysis (cf. e.g., [26]).

While the standard 2D DWT naturally outputs L^2 normalized wavelet coefficients, for scaling or fractal analysis, the L^1 normalization $d_X^{(m)}(j,k_1,k_2) = 2^{-j} D_X^{(m)}(j,k_1,k_2)$ is better suited and will hence be used from now on: Indeed, this normalization implies that scale invariance and pointwise regularity properties in data are reflected by scale invariance properties in wavelet coefficients with same scaling exponents (cf. e.g., [2,28]). More technically, pointwise Hölder regularity is defined by a local L^∞ decay condition; the wavelet normalization should therefore be of L^∞-type for the function considered and, by duality, of L^1 type for its wavelet coefficients. Using the correct normalization plays a key-role in the definition of wavelet leaders (cf. Section 2.2.1) [10].

2.1.2. Global regularity

The wavelet coefficients $d_X^{(m)}(j,\mathbf{k})$ enable to define and measure a property of X which plays a key role for fractal analysis: its global regularity h_m, defined as

$$h_m = \sup\{\epsilon : X \in C^\epsilon\}, \tag{2}$$

where $X(\mathbf{x})$ is said to belong to C^ϵ, $\epsilon \in \mathbb{R}$, iff:

$$\exists C > 0 : \ \forall j,k_1,k_2,m \ \ |d_X^{(m)}(j,k_1,k_2)| \le C 2^{j\epsilon}. \tag{3}$$

An intuitive interpretation of h_m is postponed to Section 2.3.

It follows from (3) that

$$h_m = \liminf_{2^j \to 0} \frac{\log(\sup_{m,k_1,k_2} |d_X^{(m)}(j,k_1,k_2)|)}{\log(2^j)}. \tag{4}$$

Practically, this implies that h_m can be measured by performing linear regressions of the log of the magnitudes of the largest wavelet coefficients at scales 2^j vs. the log of the scales $a = 2^j$ [28,30].

2.2. Wavelet leader multifractal formalism

The purpose of multifractal analysis is to enable image classification based on exponents characterizing the power-law behaviors of (space-averaged) space-scale quantities with respect to scale. Various such quantities were proposed in the past; however, a natural interpretation of multifractal analysis (in terms of a *multifractal spectrum*, see Section 2.3) requires it to be based on *wavelet leaders*, which we define now.

2.2.1. Wavelet leaders

Let λ_{j,k_1,k_2} denote the dyadic square

$$\lambda_{j,k_1,k_2} = [k_1 2^j,(k_1+1)2^j) \times [k_2 2^j,(k_2+1)2^j),$$

and denote by $3\lambda_{j,k_1,k_2}$ the union of λ_{j,k_1,k_2} and its eight closest neighbors,

$$3\lambda_{j,k_1,k_2} = [(k_1-1)2^j,(k_1+2)2^j) \times [(k_2-1)2^j,(k_2+2)2^j).$$

Let $\gamma \ge 0$ be defined as, with $\epsilon > 0$,

$$\gamma = \begin{cases} 0 & \text{if } h_m > 0, \\ -h_m + \epsilon & \text{if } h_m \le 0. \end{cases} \tag{5}$$

The wavelet leaders $L_X^{(\gamma)}$ are defined as [10,11,28]

$$L_X^{(\gamma)}(j,k_1,k_2) = \sup_{m,\lambda' \subset 3\lambda_{j,k_1,k_2}} |2^{\gamma j} d_X^{(m)}(\lambda')|. \tag{6}$$

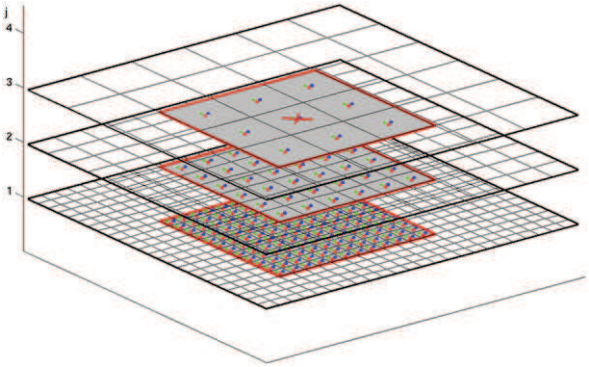

Fig. 1. Wavelet leaders. The wavelet leader $L_X(j,k_1,k_2)$, located at scale 2^j and position $(2^j x_1, 2^j x_2)$, is obtained as the largest of all wavelet coefficients located in a *narrow* spatial neighborhood and at any finer scale $2^{j'} \le 2^j$.

In other words, this means that for each node (j,k_1,k_2) of the dyadic grid, the corresponding wavelet leader $L_X^{(\gamma)}(j,k_1,k_2)$ is obtained by replacing the wavelet coefficient $d_X^{(m)}(j,k_1,k_2)$ by the largest of all the $|2^{\gamma j} d_X^{(m)}(\lambda')|$ that are located at scales finer or equal to 2^j within a small neighborhood around the position $(x_1 = 2^j k_1, x_2 = 2^j k_2)$. This construction is illustrated in Fig. 1. Mathematically, the renormalization of the wavelet coefficients by a pre-factor $2^{\gamma j}$ in Eq. (6) is equivalent to replacing the initial image by its fractional integral of order γ and amounts to increasing its global regularity exponent h_m by γ. This *renormalization* ensures that wavelet Leaders, as defined in Eq. (6) above, are mathematically well defined (cf. [28,30,1]). The precise practical selection of parameter γ is detailed in Section 2.5.

2.2.2. Multifractal formalism

Multifractal analysis consists in measuring the exponents of power-laws of the space averages of wavelet leaders across the scales available in the data. One introduces an additional parameter q and computes space averages of the q-th order of the wavelet leaders at a given scale $a = 2^j$,

$$S(2^j,q,\gamma) = \frac{1}{n_j} \sum_{k_1,k_2} L_X^{(\gamma)}(j,k_1,k_2)^q, \tag{7}$$

where n_j is the number of wavelet leaders actually computed at scale $a = 2^j$. The *scaling function* of the image is then defined as

$$\zeta(q,\gamma) = \liminf_{2^j \to 0} \frac{\log(S(2^j,q,\gamma))}{\log(2^j)}. \tag{8}$$

Note that, by construction, the scaling function is concave with respect to q [11]. Hence, it is assumed that the $S(2^j,q,\gamma)$ behave as power laws with respect to the analysis scale $a = 2^j$, in the limit of fine scales $2^j \to 0$:

$$S(2^j,q,\gamma) \sim \lambda_q 2^{j\zeta(q,\gamma)} \quad \text{when } j \to -\infty. \tag{9}$$

From a practical perspective, it is expected that this power law behavior is not limited to fine scales only, but holds over a broad range of scales. Therefore, the quantities $\zeta(q,\gamma)$ are also referred to as the *scaling exponents*. These power law

behaviors constitute the founding relation connecting the concepts of (multi)fractal and scale invariance. Moreover, it is fundamental to note that multifractal analysis requires the use of both positive and negative values of q to fully characterize the fractal properties of X. This will be further discussed in Section 2.3 (cf. e.g., [10,11,28]).

The scaling function $\zeta(q,\gamma)$ characterizes the fractal properties of the image X [28] and can be involved in any of

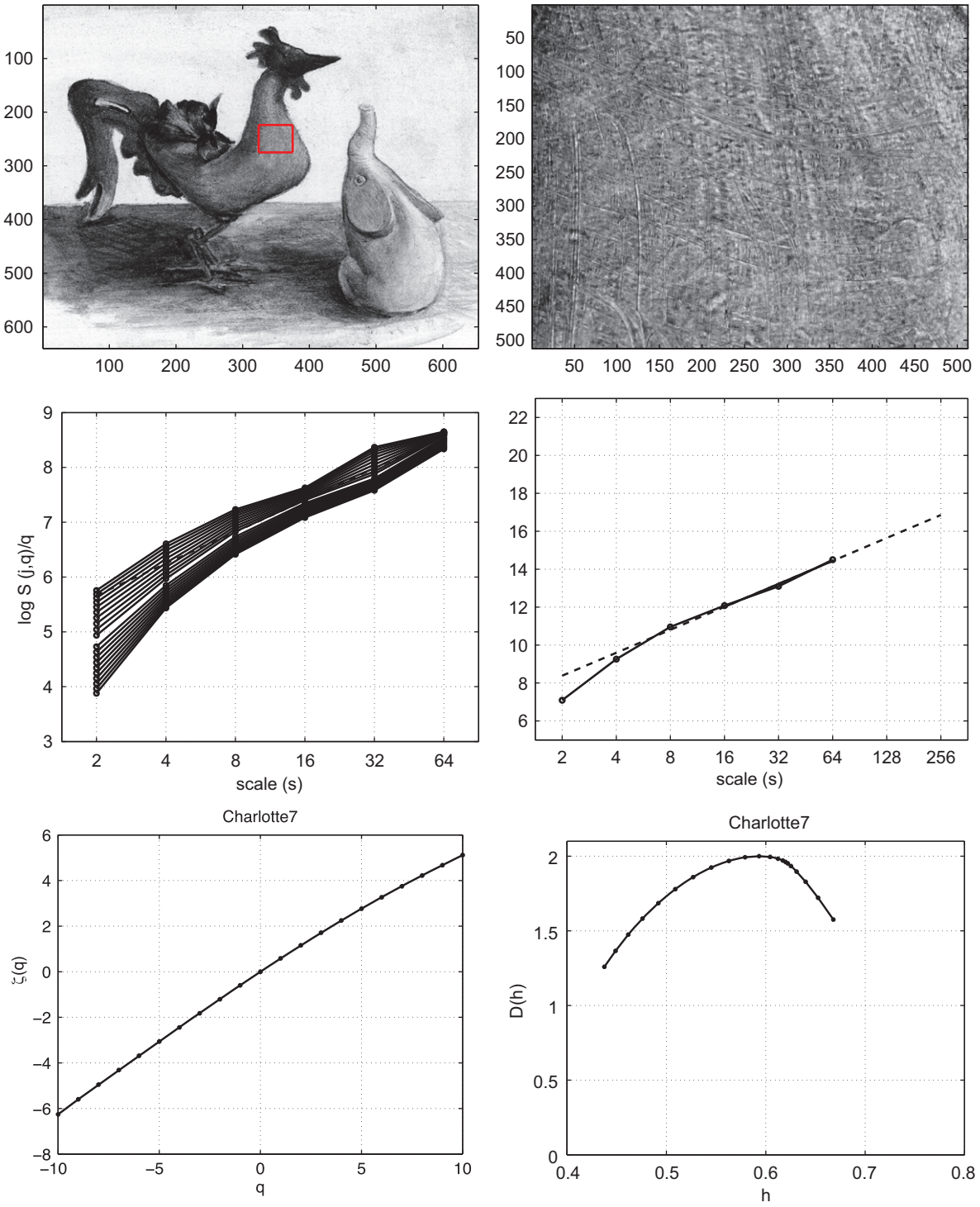

Fig. 2. Multifractal analysis—painting 7 of the Princeton experiment. From top to bottom: painting, selected patch, logscale diagrams $\log_2 S(j,q,\gamma)/q$ vs. $\log_2 2^j = j$ for numerous q's, linear regression for $q=2$, scaling function $\zeta(q)$, multifractal spectrum $D(h)$.

the usual image processing tasks, such as characterization, model selection, classification, detection, etc. This fractal characterization has been successfully adopted in image classification procedures (cf. e.g., [30]). Scaling functions obtained from one of the *Princeton* paintings and one of the Van Gogh's paintings are illustrated in Figs. 2 and 3, bottom row.

Because the practical measure of the function $\zeta(q,\gamma)$ for all q can be tedious and its use for hypothesis testing intricate, it has been proposed to use a polynomial expansion

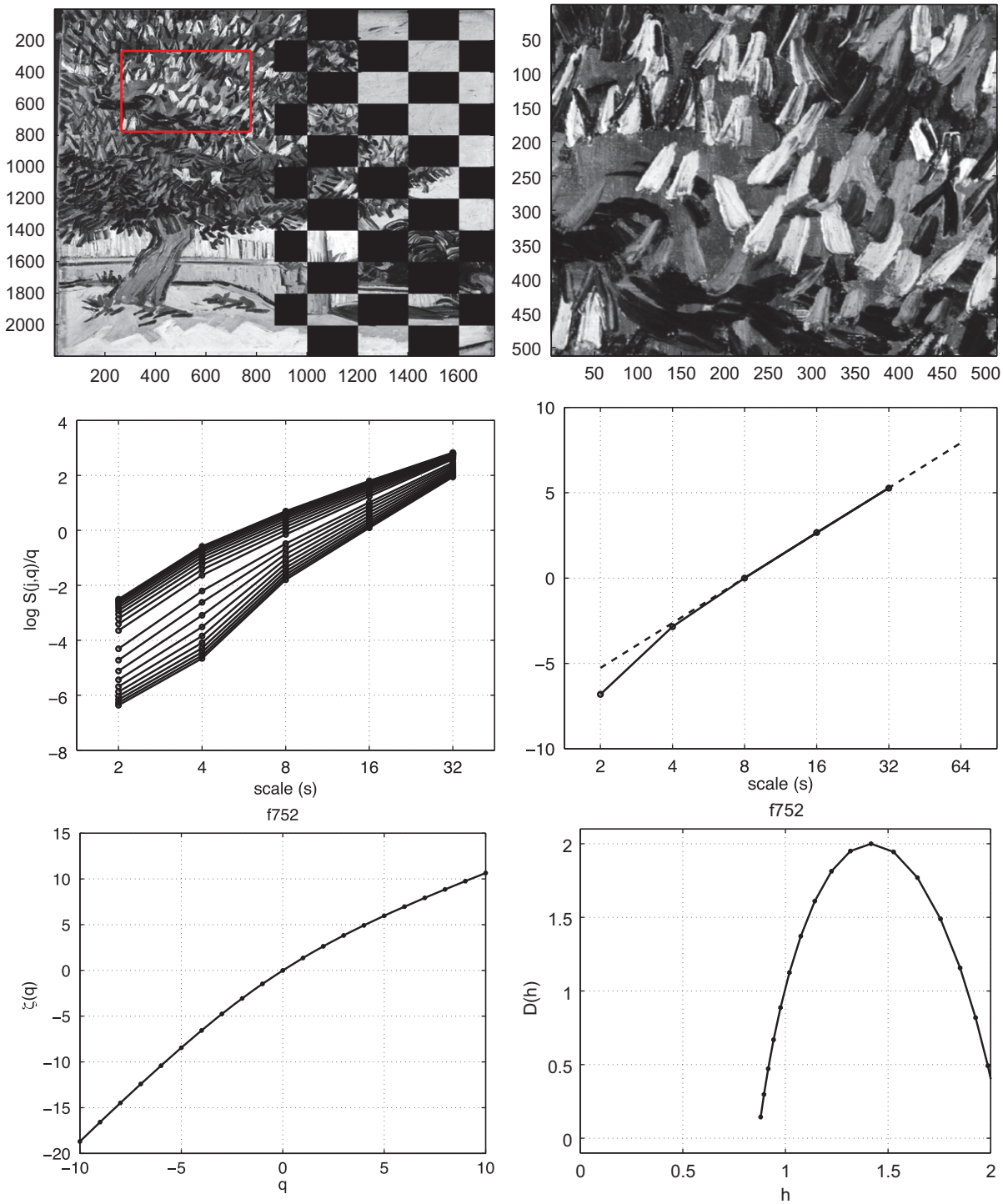

Fig. 3. Multifractal analysis—Van Gogh's Painting *f*752. From top to bottom: painting, selected patch, logscale diagrams $\log_2 S(j,q,\gamma)/q$ vs. $\log_2 2^j = j$ for numerous q's, linear regression for $q=2$, scaling function $\zeta(q)$, multifractal spectrum $D(h)$.

in the neighborhood of $q=0$ by [3,6]

$$\zeta(q,\gamma) = \sum_{p\geq 1} c_p^{(\gamma)} \frac{q^p}{p!}. \tag{10}$$

Though this expansion may not be valid in certain specific cases, its power still lies in the fact that, when well-defined, the coefficients $c_p^{(\gamma)}$ can be estimated directly (without the burden of estimating the $\zeta(q,\gamma)$ themselves), as they relate to the scale dependence of the cumulant of order p of the quantities $\ln L_X^{(\gamma)}(j,k_1,k_2)$ (cf. [3,6]). Therefore, in practice, it is often preferred to directly estimate the first values of the $c_p^{(\gamma)}$'s and work with a truncated version of the expansion equation (10) as an approximation of $\zeta(q,\gamma)$. (By concavity of the scaling function, note that $c_2^{(\gamma)} \leq 0$.)

2.3. Hölder exponents and multifractal spectrum

The wavelet leader based multifractal formalism described in the previous section constitutes one of the most powerful tools for estimating the *multifractal spectrum* of an image. It is this theoretical connection, which is now detailed, that motivates the use of wavelet leaders. However, the theoretical material developed in this section is not practically used for the analysis of the paintings described in the forthcoming sections.

Let $X:\mathbb{R}^2\to\mathbb{R}$ denote the function of interest. It is assumed that the condition $h_m>0$ holds (and hence γ is set to $\gamma=0$ in this section).

The local regularity of X at location $\mathbf{x}_0$ can be measured by comparing $X(\mathbf{x}_0)$ to a local power law behavior: $|X(\mathbf{x})-P_{\mathbf{x}_0}(\mathbf{x})| \leq C|\mathbf{x}-\mathbf{x}_0|^{\alpha}$. Here, P is a polynomial such that $deg(P)<\alpha$, $\alpha>0$ and $C>0$. The *Hölder exponent* $h(\mathbf{x}_0)$ is the largest α such that this inequality holds.

Though theoretically based on a measure of local regularity, it is essential to point out that multifractal analysis *does not* aim at providing the user with information in the form of a space dependent function $h(\mathbf{x})$, but instead with a global measure of the spatial geometry underlying the fluctuations of $h(\mathbf{x})$ along space. This is achieved via the so-called *multifractal spectrum*. It consists of the Hausdorff dimensions $\mathcal{D}$ of the sets of locations $\mathbf{x}$ for which the Hölder exponents take the same value h: $\mathcal{D}(h)=\dim_H\{\mathbf{x}:h(\mathbf{x})=h\}$. Because it is a dimension, the multifractal spectrum is confined to $0\leq\mathcal{D}(h)\leq d$. By convention, $\mathcal{D}(h)=-\infty$ for the Hölder exponents that are not present in X. In a nutshell, the key result underlying multifractal analysis is that theoretically, the Hölder exponent at a given point $\mathbf{x}$ can be recovered by linear regression (in log–log scale) of the wavelet leaders located above $\mathbf{x}$ vs. scales 2^j (see [10]). This explains why wavelet leaders are natural candidates in the construction of multifractal analysis. For theoretical introductions to multifractal analysis, the reader is referred to e.g., [10,16].

It can be shown theoretically that the Legendre transform of the scaling function $\zeta(q,0)$ provides an upper bound for the multifractal spectrum $\mathcal{D}(h)$:

$$\mathcal{D}(h)\leq\mathcal{L}(h) := \inf_{q\in\mathbb{R}}(d+qh-\zeta(q,0)). \tag{11}$$

Since experimental data are never available with an infinite resolution, the spectrum $\mathcal{D}(h)$ can never be computed for real-life images. Thus, in practice, $\mathcal{L}(h)$ is the only quantity that can be estimated. Therefore, with slight abuse of language, one often refers to $\mathcal{L}(h)$ as the multifractal spectrum. Also, the polynomial expansion (10) can be recast for $\mathcal{L}(h)$. Its truncation to the first two expansion terms, valid for h in the vicinity of c_1, is given by (cf. [27] for a complete formula)

$$\mathcal{L}(h)\simeq d+\frac{c_2}{2}\left(\frac{h-c_1}{c_2}\right)^2. \tag{12}$$

This approximation shows that c_1 corresponds to the value of h where $\mathcal{L}(h)$ is maximal, hence to the most typical regularity exponent h observed in X, and $-c_2$ essentially measures the dispersion of the values of h encountered in X (explaining why it is sometimes referred to as the *strength* of the multifractality). The Legendre transform used above (cf. Eq. (11)) indicates that both positive q's (capturing the smallest h's) and negative q's (capturing the largest h's) must be used in order to obtain the full curve $\mathcal{L}(h)$. Moreover, note that the global regularity exponent h_m, when positive, corresponds to the smallest value of h that exists in X (i.e., the leftmost point of $\mathcal{L}(h)$ for which $\mathcal{L}(h)\neq-\infty$).

Multifractal spectra obtained from one of the *Princeton* paintings and one of Van Gogh's paintings are displayed in Figs. 2 and 3 bottom row.

2.4. Estimation procedures

The procedures to estimate the $\zeta(q,\gamma)$, the $c_p^{(\gamma)}$ and the function $\mathcal{L}(h)$ from data have been presented and studied in detail in [28–30], and are hence not further recalled here. In essence, they rely on weighted linear regressions in suited log–log diagrams, as illustrated in Figs. 2 and 3 (middle row) for one of the *Princeton* paintings and one of Van Gogh's paintings.

2.5. The role and selection of parameter γ

Multifractal analysis makes sense in terms of fractal or scaling properties only for functions for which $h_m>0$. This limitation is alleviated by the introduction of the parameter γ in Eq. (6): Indeed, as mentioned in Section 2.2, when analyzing an image for which $h_m<0$, one could first perform a fractional integration of order larger than $-h_m$ (which ensures that the global regularity exponent of the integrated image is positive) and then apply the wavelet leader multifractal formalism (with $\gamma=0$) to it. Alternatively, one can avoid actual computation of the fractional integral and instead apply the wavelet leader multifractal formalism with $\gamma>-h_m$ directly to the original image. It has been shown theoretically that both analyses yield the same multifractal properties (cf. [28,29] for details).

In practice, the multifractal parameters associated with X can be related to those computed using various choices of $\gamma>h_m$ as follows (cf. [30]):

$$\zeta_X(q)=\zeta(q,\gamma)-\gamma q, \tag{13}$$

$$c_{X,1}=c_1^{(\gamma)}-\gamma, \tag{14}$$

$$c_{X,p}=c_p^{(\gamma)},\quad p\geq 2, \tag{15}$$

$$\mathcal{L}_X(h) = \mathcal{L}^{(\gamma)}(h-\gamma). \quad (16)$$

Given that h_m needs to be estimated, a rule of thumb for comparison or classification of several images is to choose γ as the smallest semi-integer value ensuring $\gamma + h_m > 0$ for all images under analysis.

3. Original vs. replica: the Princeton experiment

Appealing though it may be, applying multifractal analysis immediately and blindly to masterpieces, such as Van Gogh's paintings, with the aim of, e.g., performing forgery detection or classification according to given artistic periods is difficult since the correct answers are often still under debate among conservators and art historians. Furthermore, the questions raised by conservators and art historians must first find a relevant formulation in an Image Processing language. Therefore, we instead begin with testing multifractal analysis on the *Princeton experiment* data.

3.1. The Princeton experiment

The *Machine Learning and Image Processing for Art Investigation Research Group* at Princeton University (cf. www.math.princeton.edu/ipai/index.html) had the brilliant idea of setting up a *scientific* art investigation experiment. It is described in detail at www.math.princeton.edu/ipai/datasets.html and in [9,15]: Charlotte Caspers, then an art conservation student from Stichting Restauratie Atelier Limburg specializing in art reconstruction, was proposed to perform a series of seven paintings using different materials (various brushes, canvas, paints). All of them are *small* ($\simeq 15 \times 15$ cm^2) and represent indoor environment still life subjects. After a delay of two weeks, she was asked to produce, under the same conditions and using the same materials, replicas that were as close as possible to her originals. Originals and replicas were scanned at very high resolution (800 dpi) enabling to analyze the very fine scales of the texture (as a pixel essentially represents 32×32 μm^2). The paintings are described in Table 1 and plotted in Fig. 4. The Princeton group is gratefully acknowledged for making the material of this experiment available to other research teams.

Table 1
The Princeton experiment—discriminating original from replica. Soft brushes (S) are sable or synthetic, hard brushes (H) are flat hog hair. Replicas have textures which are globally more regular than those of originals. For Paintings 1–3, this is well detected by both the PairWise (PW) and the Non-PairWise (NPW) tests. While this is also the case for Paintings 5 and 7, only the PairWise (PW) tests, comparing patches with same locations on original and replica, are discriminative.

Pair	Ground	Paint	Brushes	Pixel	Discr.
1	CP Canvas	Oils	S & H	6272×6528	PW/NPW
2	CP Canvas	Acrylics	S & H	6272×6528	PW/NPW
3	Smooth CP Board	Oils	S & H	6272×6528	PW/NPW
4	Bare Linen Canvas	Oils	S	3200×6144	–
5	Chalk and Glue	Oils	S	3328×4608	PW
6	CP Canvas	Acrylics	S	3456×5504	–
7	Smooth CP Board	Oils	S	6400×6528	PW

3.2. Multifractal properties

To analyze and assess fractal properties in paintings, small patches of homogeneous textures of $N \times N$ pixels are manually selected. Then, the wavelet leader multifractal formalism described in Section 2 is applied to each of them. Structure functions $S(j,q,\gamma)$ are depicted in Figs. 2 and 3 and display the power law behavior postulated in Eq. (9) satisfactorily well for a range of values of q around 0 (here, $q \in [-5;5]$ and $N=1024$). These power laws hold for all seven paintings, for both originals and replicas, for many different patches at various positions in the painting (bird, bag, upper background, lower background, etc.). Their existence confirms that the fractal (or scaling) properties in these paintings can be regarded as relevant features to describe their textures. Other figures, in the spirit of Fig. 5, are not reported here for the sake of space and are available upon request.

An important aspect of (wavelet leader) multifractal analysis lies in the fact that the range of scales $a \in [a_{min}, a_{max}]$ within which scaling behavior as in Eq. (9) holds, is selected a posteriori from visual inspection of the log–log diagrams, such as those in Fig. 2, by the expert performing the analysis (assisted by statistical procedures, cf. [25]). Therefore, the selection of the relevant range of scales is not an a priori and arbitrary choice but constitutes per se an important output of the analysis: it provides information on the scales in actual units within which fractal properties hold. For the Charlotte Casper paintings, it can be estimated that scaling holds over a decade, within scales ranging from 0.5×0.5 to 5×5 mm^2. This shows that the observed scaling properties are related to fine details of the various textures in the paintings and not to the (larger scale) shapes of the represented subjects.

Furthermore, patches of the same location on both original and replica do not share the same scaling properties. This is illustrated in Fig. 5, where the scaling functions and the multifractal spectra significantly differ. Interestingly, it is found that the multifractal spectra estimated from replicas tend to be systematically shifted to the right on the Hölder exponent axis, as compared to those measured on originals. Technically, this is effectively measured on c_1, which estimates the position of the maximum of the multifractal spectrum: It is often observed that $c_1^{(\text{replica})} > c_1^{(\text{origin.})}$. Consistently, it is observed that $h_m^{(\text{replica})} > h_m^{(\text{origin.})}$. Both these observations clearly indicate that systematically, the textures of the replicas are *globally more regular* and *smoother* than those of the original paintings.

3.3. Results

3.3.1. Test procedure set-up

This section aims at deciding, by means of statistical procedures, whether the differences between the multifractal parameters estimated on replicas and originals we observed and discussed in the previous section are statistically significant or not.

A key point in the analysis underlying the above observations (cf. Section 3.2) resides in the fact that multifractal parameters were estimated for well-chosen patches of homogeneous textures (the bird, as in the example illustrated

Fig. 4. The Princeton experiment. The seven originals, numbered 1–7 hereafter.

in Fig. 2, the bag, the backgrounds, etc.). This manual selection of patches requires a human/expert decision and cannot be easily automated. Here, we chose instead to split each painting blindly into adjacent non-overlapping patches of $N \times N$ pixels. Then, the wavelet leader based multifractal formalism is applied to each patch independently. Following the preliminary analysis described above, the scaling range is fixed to scales ranging from 0.5×0.5 to $5 \times 5\,\mathrm{mm}^2$. In the results reported below, patch sizes $N = 2^9, 2^{10}, 2^{11}$ have been used and yield consistent conclusions. Tables are given for $N = 2^{10}$.

Along another line, the digitized paintings are provided in the form of three 8 bit matrices, which correspond to the RGB channel outputs supplied by the scanner, respectively. Systematically, these three channels have been transformed into a single Intensity gray-level image I, and into three channels corresponding to the classical HSL (Hue, Saturation, Lightness) representation system for colors (cf. e.g., en.wikipedia.org/wiki/HSLandHSV for the exact definitions of the transformation RGB$\rightarrow$I and RGB$\leftrightarrow$HSL). For each patch of each original and replica, these seven instances (RGB, I, HSL) were analyzed independently.

Three characteristic multifractal parameters have been systematically retained for the test procedures: h_m, c_1 and c_2. The results shown here are obtained using the minimal compact support orthonormal Daubechies wavelet ψ with $N_\psi = 2$ vanishing moments [5]. It has been checked that results are consistent when N_ψ is increased. A value $\gamma = 1$ is found to be sufficiently large to ensure positive global regularity for all paintings and patches.

To test whether changes between multifractal parameter estimates for original and replica are significant, a set of classical non-parametric hypothesis tests is applied and p-values are computed for the null hypothesis that no change is observed between original and replica. Two categories of tests were used. PairWise tests (SignTest and SignRank) compare estimates obtained for patches of the same locations on original and replica. Non-PairWise tests (Wilcoxon RankSum) compare globally the vectors containing multifractal attribute estimates for all patches of the original and replica, respectively, without taking the locations of the patches into account. They are hence far more demanding, since they could be used to compare two sets of paintings which are not originals and copies or replicas thereof. This setting is much more likely to be of interest in practice. It corresponds, for instance, to the situation where a reference set of paintings that are indisputably attributed to a master (or a period of creation) is used to test a set of paintings that are questionably attributed to this master (or a period of creation).

The level of significance of the tests is, as is classically done, set to 0.05 (i.e., differences are regarded as

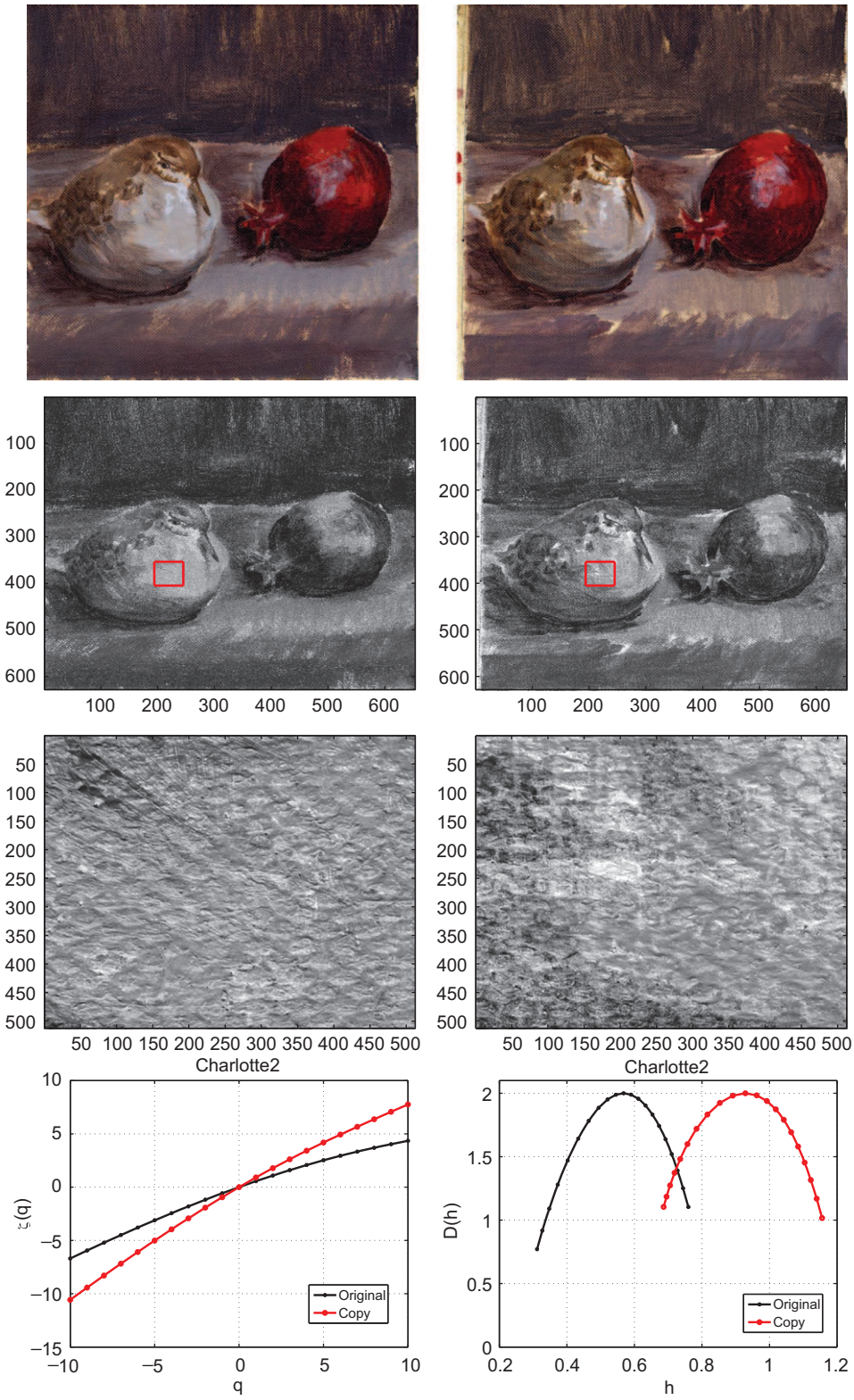

Fig. 5. Multifractal analysis. Three first lines: original (left) and replica (right). Last line: estimated multifractal attributes, original (black) and replica (red). (For interpretation of the references to color in this figure legend, the reader is referred to the web version of this article.)

statistically significant whenever $p \leq 0.05$, and the test has a 5% level of chances of incorrectly deciding so). Tests are applied to both the multifractal parameters estimated from all seven channels, and to those of the L channel only (hence to those of a single gray-level image).

3.3.2. Results

In Fig. 6, multifractal parameter estimates of originals and replicas are compared by means of box-plots. The p-values resulting from the different tests are reported in Table 2. Careful reading of this table and figure enables to

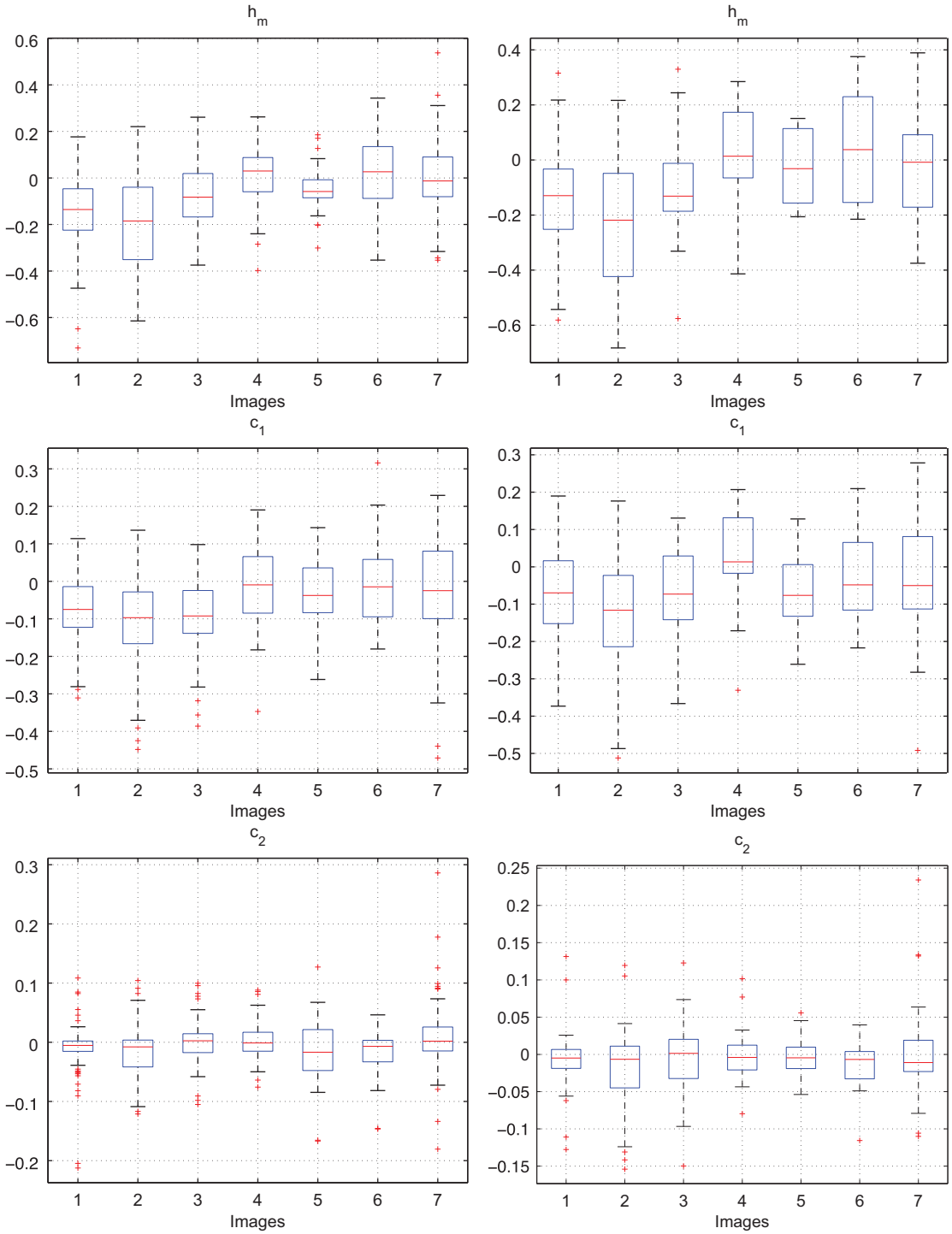

Fig. 6. Differences in multifractal parameters for the seven paintings. Top: h_m, middle: c_1, bottom: c_2; Left: All seven channels, right: Luminance L channel only.

Table 2
p-Values. For each seven sub-tables (corresponding to the seven images), the *p*-values correspond to the PairWise SignTest (left), PairWise RankTest (centerleft), Non-PairWise Wilcoxon RankSum (centerright:). The Right pair of columns reproduces the mean value of the difference between original and replica. In each pair of columns, the left column corresponds to the test applied to all seven channels, while the right column shows results for the test applied to the Luminance channel only.

	All	Lum.	All	Lum.	All	Lum.	All	Lum.
1-Channel								
h_m	0.00	0.00	0.00	0.00	0.00	0.03	−0.14	−0.15
c_1	0.00	0.03	0.00	0.01	0.00	0.14	−0.07	−0.06
c_2	0.15	0.62	0.01	0.20	0.02	0.28	−0.01	0.01
2-Channel								
h_m	0.00	0.24	0.00	0.00	0.00	0.00	−0.20	−0.23
c_1	0.00	0.00	0.00	0.00	0.00	0.02	−0.11	−0.12
c_2	0.00	0.41	0.00	0.10	0.00	0.03	−0.02	0.02
3-Channel								
h_m	0.00	0.00	0.00	0.00	0.01	0.08	−0.07	−0.10
c_1	0.00	0.03	0.00	0.00	0.03	0.21	−0.06	−0.08
c_2	0.73	1.00	0.58	0.74	0.53	0.54	−0.00	0.00
4-Channel								
h_m	0.21	0.48	0.44	0.31	0.58	0.87	0.01	0.02
c_1	0.39	0.48	0.47	0.40	0.90	1.00	0.01	0.01
c_2	0.00	0.48	0.06	0.81	0.21	0.87	−0.01	0.01
5-Channel								
h_m	0.01	0.39	0.02	0.38	0.38	0.72	−0.05	−0.01
c_1	0.00	0.15	0.00	0.06	0.24	0.87	−0.05	−0.02
c_2	0.08	0.77	0.02	0.62	0.49	0.98	−0.02	0.00
6-Channel								
h_m	0.60	1.00	0.32	0.33	0.39	0.94	0.03	0.02
c_1	0.60	0.60	0.07	0.39	0.79	0.94	−0.02	−0.01
c_2	0.04	0.04	0.01	0.11	0.37	0.61	0.15	0.01
7-Channel								
h_m	0.00	0.87	0.01	0.50	0.29	0.75	−0.03	−0.02
c_1	0.01	0.24	0.00	0.31	0.13	0.77	−0.05	−0.03
c_2	0.54	0.24	0.98	0.57	0.26	0.90	0.00	−0.00

make the following observations:

- When significant, changes in c_1 and h_m are observed to systematically occur jointly and with larger values for replicas as compared to originals.
- Parameter c_2 is rarely found discriminant and when it is, changes in c_2 are not systematical in the same direction.
- For Paintings 1–3, both PairWise and Non-PairWise tests detect significant changes, be they applied to All-Channels or to Luminance only.
- For Paintings 5 and 7, discrimination is only achieved for PairWise tests applied to All-Channels.
- For Paintings 4 and 6, no change between original and replica is detected.

Such observations induce the following conclusions, which are summarized in Table 1:

- *Multifractal properties*. When significant changes are found, the multifractal spectra computed from the textures of the replicas appear globally shifted to the right, with quasi no deformation: the change in h_m (the left-most point of the spectrum) is comparable to the change in c_1 (the location of its maximum) and c_2 (related to its width) is not changed. Therefore, the textures in replicas systematically are globally more regular than those of the originals, but they show neither a larger nor a smaller variability around this global regularity. Let us also recall the important fact that fractal properties are observed for scales ranging from 0.5×0.5 to 5×5 mm^2. Hence, the fractal properties observed in this data set may be tentatively related to brushstrokes, though there is no objective consensus on which scales relate to which characteristics of paintings (cf. [7,23] for discussions on these issues).
- *Painting properties*. While discriminations between replicas and originals are clear and obvious for the three first paintings whose common feature is the use of Soft and Hard brushes, discrimination is not or barely achieved for paintings for which only Soft brushes were used. Consequently, a natural conclusion is to attribute this difference to the brushes actually used. The fact that the PairWise tests yield detection for paintings 5 and 7 remain to be interpreted. Furthermore, the reasons why no discrimination is achieved for paintings 4 and 6 remain to be understood. For these paintings, scaling and fractal properties are observed which are qualitatively similar to those of the other paintings (as illustrated in Fig. 7) yet are not discriminant. Note that for paintings 4 and 6 a strong canvas structure is present and may constitute the dominant feature of the texture (cf. Fig. 7). Because it exists for both the original and the replica, it may prevent discrimination.[1]

4. Van Gogh's paintings multifractal properties

4.1. The Image Processing for Art Investigation research project

Let us now turn to the analysis of Van Gogh's paintings. In the framework of the *Image Processing for Art Investigation* research project initiated by R. Johnson (Cornell University) and I. Daubechies (Princeton University; cf. digitalpaintinganalysis.org) the Van Gogh Museum and the Kröller-Müller Museum (The Netherlands) made available a set of digitized versions of Van Gogh's paintings and of his contemporaries. These copies were obtained using a scanning resolution of 200 dpi and are *checkerboarded* on their right-half side, so that only the left-half is actually available for analysis. In order to investigate the potential of image processing tools for art investigation, a series of stylometry challenges was set up under the supervision of R. Johnson, J. Coddington

[1] During the revision process, experts of the field kindly pointed to us that for paintings 1–3, the artist had first painted the whole canvas, while this turns out not to be the case for paintings 4–7. Moreover, colors used in paintings 4–7 are much *lighter* and *clearer* than those in paintings 1–3. These suggest that for paintings 1–3 the analyzed textures correspond to the *hand* of the artist, while for paintings 4–7, they rather result from a mixture on canvas textures and artist hand style, hence explaining less satisfactory results. Analysis that removing the canvas effect is currently under investigations. These spontaneous expert readers are gratefully acknowledged.

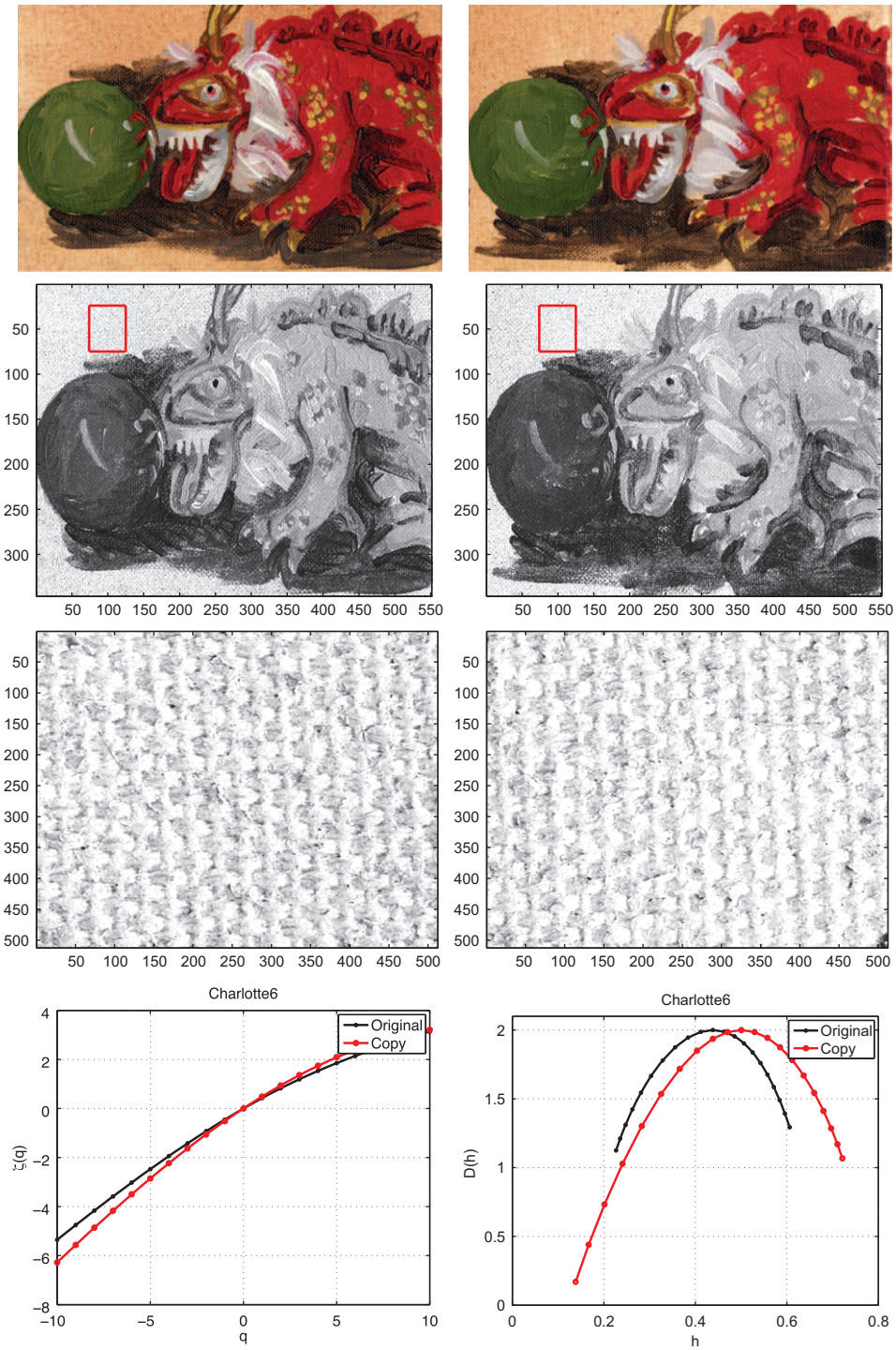

Fig. 7. Multifractal analysis. Three first lines: original (left) and replica (right). Last line: estimated multifractal attributes, original (black) and replica (red). (For interpretation of the references to color in this figure legend, the reader is referred to the web version of this article.)

(MoMA, New York) and L. van Tilborgh (Van Gogh Museum, Amsterdam). These challenges are described in detail at www.digitalpaintinganalysis.org/Challenges.htm. In the present contribution, we chose to illustrate the results obtained on the *dating* and *authenticity* challenges, which are summarized below.

4.2. Methodology

Because paintings naturally consist of different textures, they are not analyzed globally. Instead, fractal property analysis is based on the manual selection of small patches of $N \times N = 512 \times 512$ pixels for each

painting (roughly $5 \times 5\ \mathrm{cm}^2$). The wavelet leader multifractal formalism, described in Section 2, is applied to each of the seven channels of the patches (RGB, HSL, Intensity, cf. Section 3.3.1) and the corresponding multifractal attributes $\zeta(q)$,$D(h)$,h_m,c_1,c_2 are computed. Results shown here are obtained using the Daubechies wavelet with $N_\psi = 2$ and are consistent with those obtained when N_ψ is increased. From preliminary analysis, we conclude that $\gamma = 0.5$ is sufficient to guarantee positive global regularity for each painting (cf. Sections 2.1.2 and 2.5).

The choice of a patch for each single painting is based on the following criteria:

- *Homogeneity of texture*: Patches are manually located on pieces of texture that appear homogeneous for all seven channels in order to limit the presence of large-scale coherent structures and heterogeneity (such as the arms of the windmill in f503, or a combination of background and subject) which could potentially obstruct the analysis. Note that different channels of the same patch may reveal very different textures and structures (cf. e.g., the Red Channel of painting f452 in Fig. 9, and its Saturation Channel in Fig. 10). Moreover, care has been taken to locate the patches on regions of the painting which may be assumed to have been subject to similar techniques, combinations of brushes, etc. (e.g., the heads of flowers in a bouquet, or a part of the background).
- *Scaling and multifractal properties*: The choice of patch locations is guided by the quality of the observed scaling properties, involving careful inspection of the wavelet coefficient analog of Eq. (7) prior to fractional integration and monitoring theoretical constraints on parameter estimates (for instance, $c_2 \leq 0$). Furthermore, estimates are required to be stable with respect to small changes in the patch location.

The lower scanning resolution (as compared to that in the Princeton Experiment) makes it more difficult to decide accurately on the range of scales to be involved in estimation. Nevertheless, scaling properties are overall found to systematically hold for scales ranging from $0.5 \times 0.5\ \mathrm{mm}^2$ to $5 \times 5\ \mathrm{mm}^2$, for all paintings in both challenges, and may hence again be tentatively related to brushstrokes.

While some of the paintings do not leave much freedom for locating a patch because of their limited size (e.g., f441 and s448, cf. Figs. 8 and 12, respectively), others do (e.g., *f*297, *f*392 or *f*411). For these, different patches could be selected for analysis. A careful inspection suggests that the multifractal attributes obtained on different patches from a single painting are consistent and remain within the natural statistical fluctuation of the estimation procedures. This is illustrated in Fig. 9, where analysis results for three patches of painting f452 are compared.

4.3. Dating challenge

4.3.1. Description

Van Gogh, while in France, had two major periods of creation: one in Paris (ending early 1888) and one later on in the Provence. While a number of his paintings are unambiguously attributed to the Paris or to the Provence periods, the decision for other paintings of the master is still under debate amongst experts and art historians. Investigations by art experts often rely on a number of material and stylometric features (density of brush strokes, size or scale of the brush strokes, thickness of contour lines, layers, colors, etc.). In an attempt to investigate the potential benefits of computer-based image processing procedures for assisting art experts in painting analysis, two sets of height paintings each from the Paris and Provence period are given as benchmark references, together with three paintings whose dates of creation are unknown. The low resolution digitized copies of Van Gogh's masterpieces in

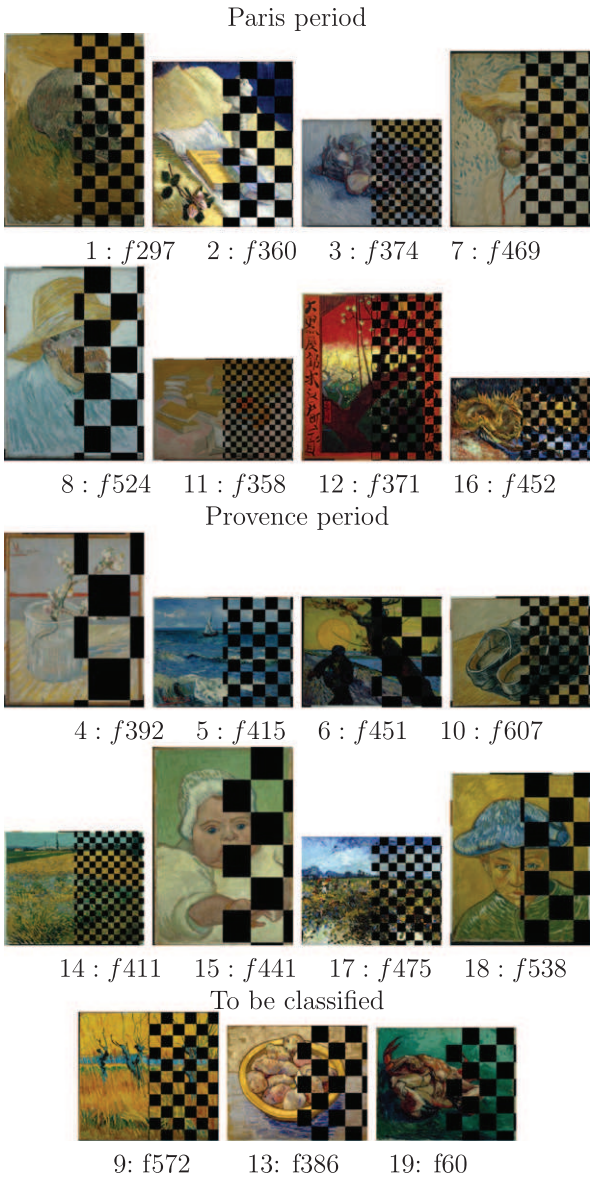

Fig. 8. Dating challenge: Provence vs. Paris periods. Eight paintings from the Paris period (top), eight paintings from the Provence period (middle), three paintings to be classified.

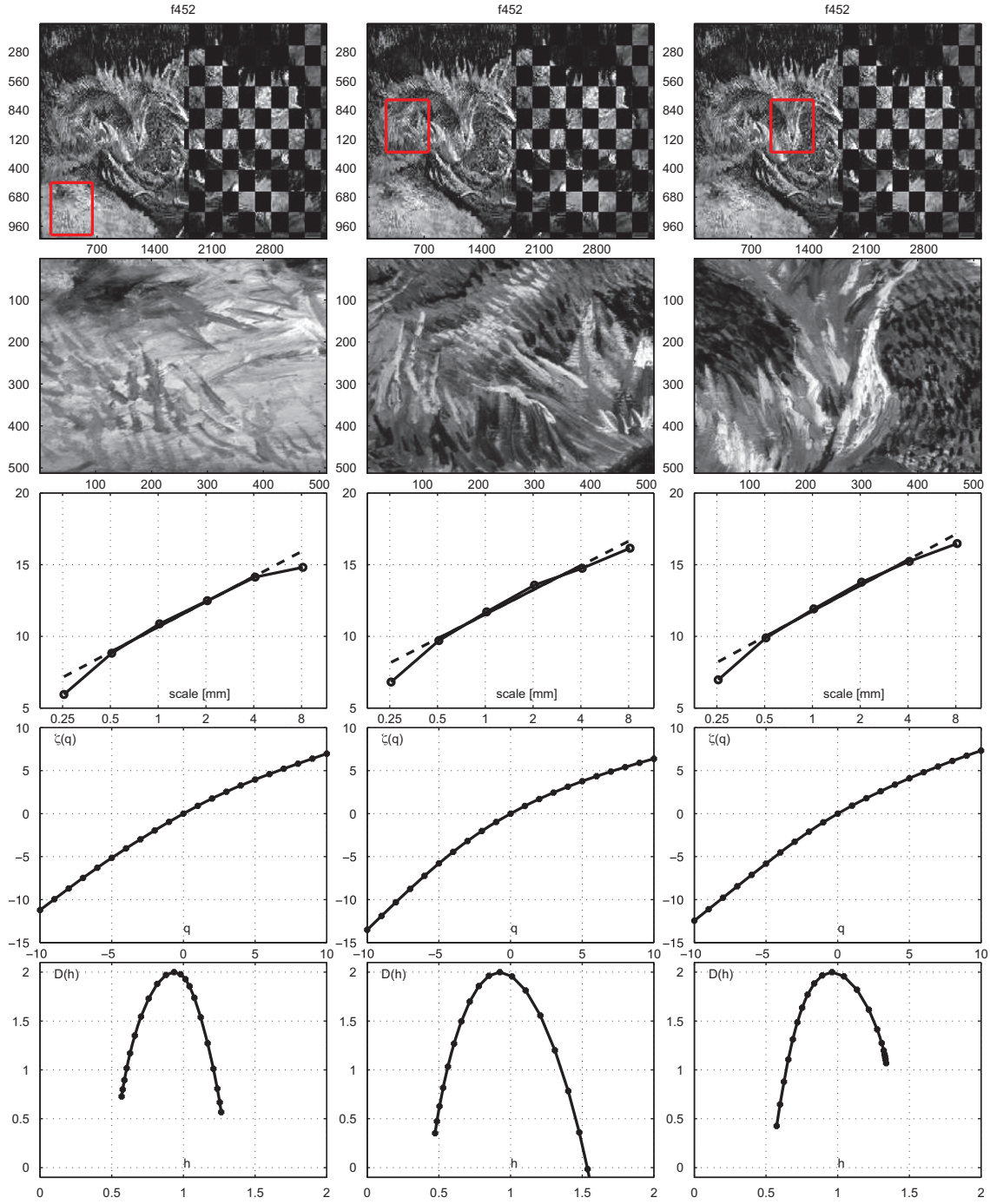

Fig. 9. Multiple patches from one single painting. The multifractal spectra computed on three different patches extracted from the Red Channel of Van Gogh's Painting *f*452 from the Paris period suggest that estimates from the three patches of visually different textures are consistent. The precise values for the multifractal attribute triple (c_1,c_2,h_m) are (from left to right): (0.93,−0.051,0.050), (0.93,−0.081,−0.051), (0.96,−0.076,−0.007).

these three sets are shown in Fig. 8 (nomenclature corresponds to the Van Gogh Museum catalog).

4.3.2. Results

In Fig. 10, logscale diagrams, scaling functions and multifractal spectra are illustrated for the Saturation Channel of one (arbitrarily selected) painting per class (Paris, Provence and Unknown). They indicate that the painting from the Provence period may show globally less regularity than the Paris period.

In an attempt to further quantify this preliminary observation, we chose to analyze the reduced set c_1,c_2,h_m of wavelet leader based multifractal attribute estimates in more detail. Because recourse to machine learning techniques

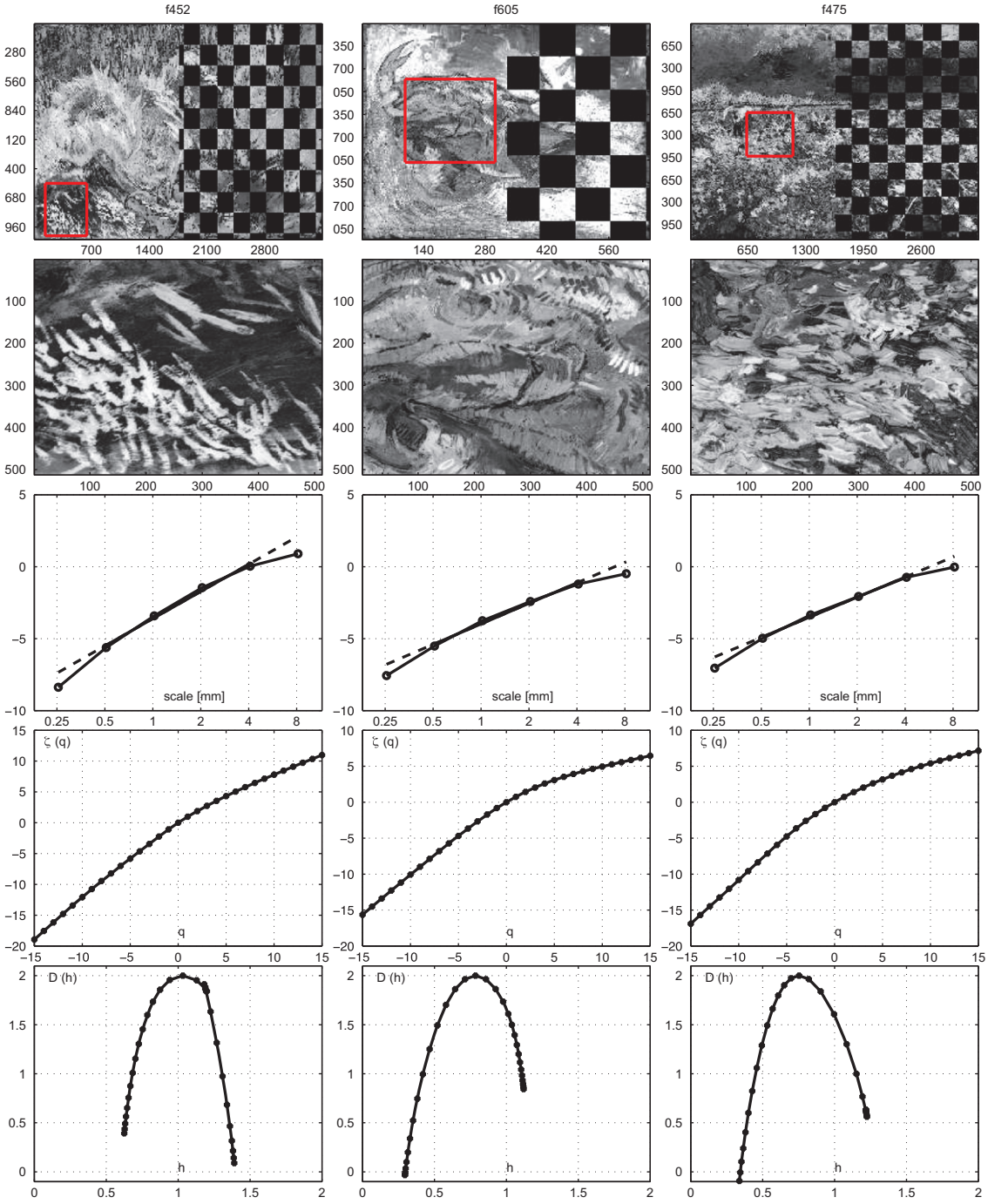

Fig. 10. Dating challenge: Paris vs. Provence periods. Multifractal spectra computed on patches extracted from the Saturation Channel of Van Gogh's Paintings: Paris period (*f*452, left), Provence period (*f*475, right), to be classified (*f*605, middle).

(such as support vector machines) does not make any sense for the 19(=8+8+3) subjects living in a 42(=7∗3∗2) dimensional space, we instead manually inspect a large collection of 2D projections of this space. The most convincing discrimination is obtained with parameter h_m computed from the Red-Channel and c_1 from the Saturation-Channel, the latter being particularly discriminant (cf. Fig. 11). Interestingly, art historians use saturation in colors one of the features to discriminate the Paris and Provence periods (cf. www.digitalpaintinganalysis.org/Challenges.htm). Note, however, that multifractal analysis does not discriminate levels of saturation but instead the regularity of the texture in the Saturation-Channel. This projection supports the above observation: textures in Van Gogh's during the Paris period appear to be more regular, which may indicate more regularity in the brushstrokes themselves. These results are

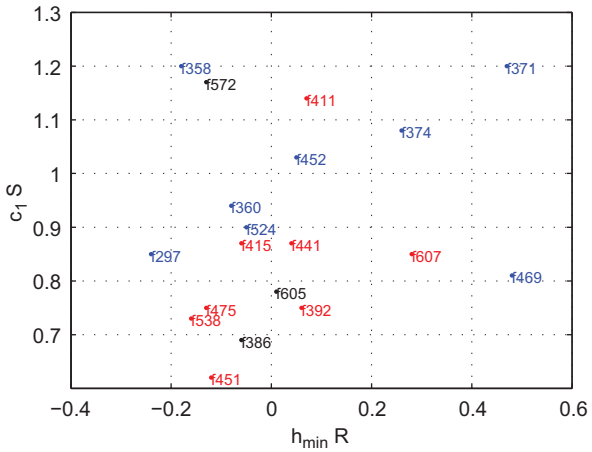

Fig. 11. Dating challenge: Paris vs. Provence periods. Plot of h_m computed from the Red Channel vs. c_1 from the Saturation Channel, suggesting that paintings *f*386 and *f*605 are closer to the Provence period cluster (red), while painting *f*572 is closer to the Paris period cluster (blue). (For interpretation of the references to color in this figure legend, the reader is referred to the web version of this article.)

consistent with findings in [12], where larger wavelet coefficients at fine scales (hence more irregularity) are observed for non-Van Gogh's than for Van Gogh's paintings. Also, the results obtained here suggest that paintings *f*386 and *f*605 are closer to the Provence period cluster (red), while *f*572 is closer to the Paris period cluster (blue). However, it must be noted that when relying on fractal properties, painting *f*411 from the Provence period would be incorrectly attributed to the Paris period.

4.4. Authenticity challenge

4.4.1. Description

In this challenge, digitized copies of four paintings by Van Gogh and four paintings by his contemporaries are provided, along with one painting that is labelled unknown and proposed for classification. The latter painting is a known contemporary copy of an original Van Gogh painting. However, the original Van Gogh is not in the available data set, hence preventing us from performing comparisons similar to those conducted on the Princeton experiment data. Experts state that the colors of the copy have remained closer to the original colors than those of the painting by the master. Essentially, their distinction between true Van Gogh's and non-Van Gogh's is based on a careful analysis of Van Gogh's brushstroke referred to as *vigourous*, with non-overlapping and neatly defined strokes, as opposed to those of his contemporaries which are found to be either too academic and regular, or too messy and irregular (cf. www.digitalpaintinganalysis.org/Challenges.htm see also [13,24], where brushwork texture and numerical brushstroke features are employed for authentificating Van Gogh's paintings).

The challenge consists in devising numerical features which distinguish the two test sets and which enable to associate the test painting with one or the other group. The nine paintings are shown in Fig. 12.

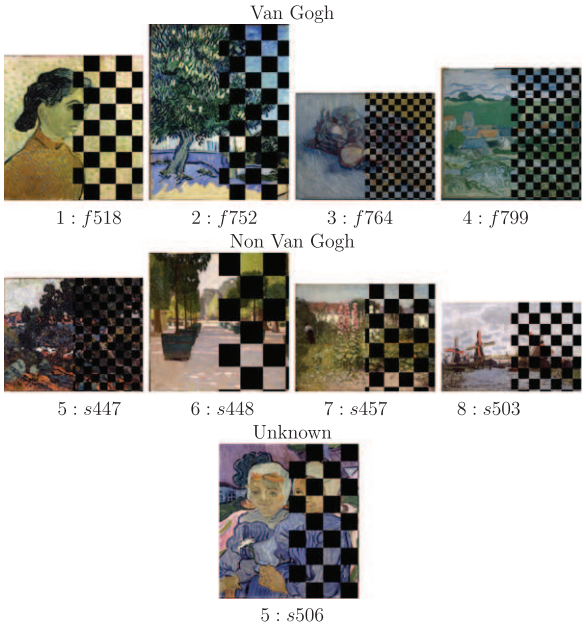

Fig. 12. Authenticity challenge: Van Gogh's vs. non-Van Gogh's paintings. Four paintings from Van Gogh (top), four paintings not from Van Gogh (middle), and the painting to be classified.

4.4.2. Results

Fig. 13 plots logscale diagrams, scaling functions and multifractal spectra obtained on the Red Channel of one arbitrarily selected painting for each of the reference classes, and of the painting whose label is to be determined.

A careful inspection of the multifractal spectra leads us to suggest that Van Gogh's paintings tend to be globally more regular. Systematic estimation of the h_m,c_1,c_2 parameters on the seven channels of the nine paintings and manual analysis and 2D projections, as described for the dating challenge, reveal that the Saturation and Red Channels are most discriminant between the two sets. This analysis indicates that the non-Van Gogh paintings have smaller values for h_m and c_1 and hence appear to be overall more irregular (cf. Fig. 14). These 2D projections also suggest, however, that the painting *s*506 under investigation is closer to the authentic Van Gogh paintings cluster than to the Non-Van Gogh cluster. This incorrectly contradicts the experts' decision, but may indicate that the copyist was successful here in reproducing Van Gogh's brushstroke regularity.

5. Conclusions and perspectives

This contribution illustrates the potential and possibilities of wavelet leader based multifractal analysis of digitized paintings for assisting art investigation.

At the technical level, this work shows that for well assessing the relevance of fractal properties, as well as the range of scales where they can be regarded as relevant, classical wavelet coefficients must be used to complement the wavelet leader multifractal formalism. Also, multifractal analysis cannot be applied blindly to arbitrary pieces of images or paintings since they usually

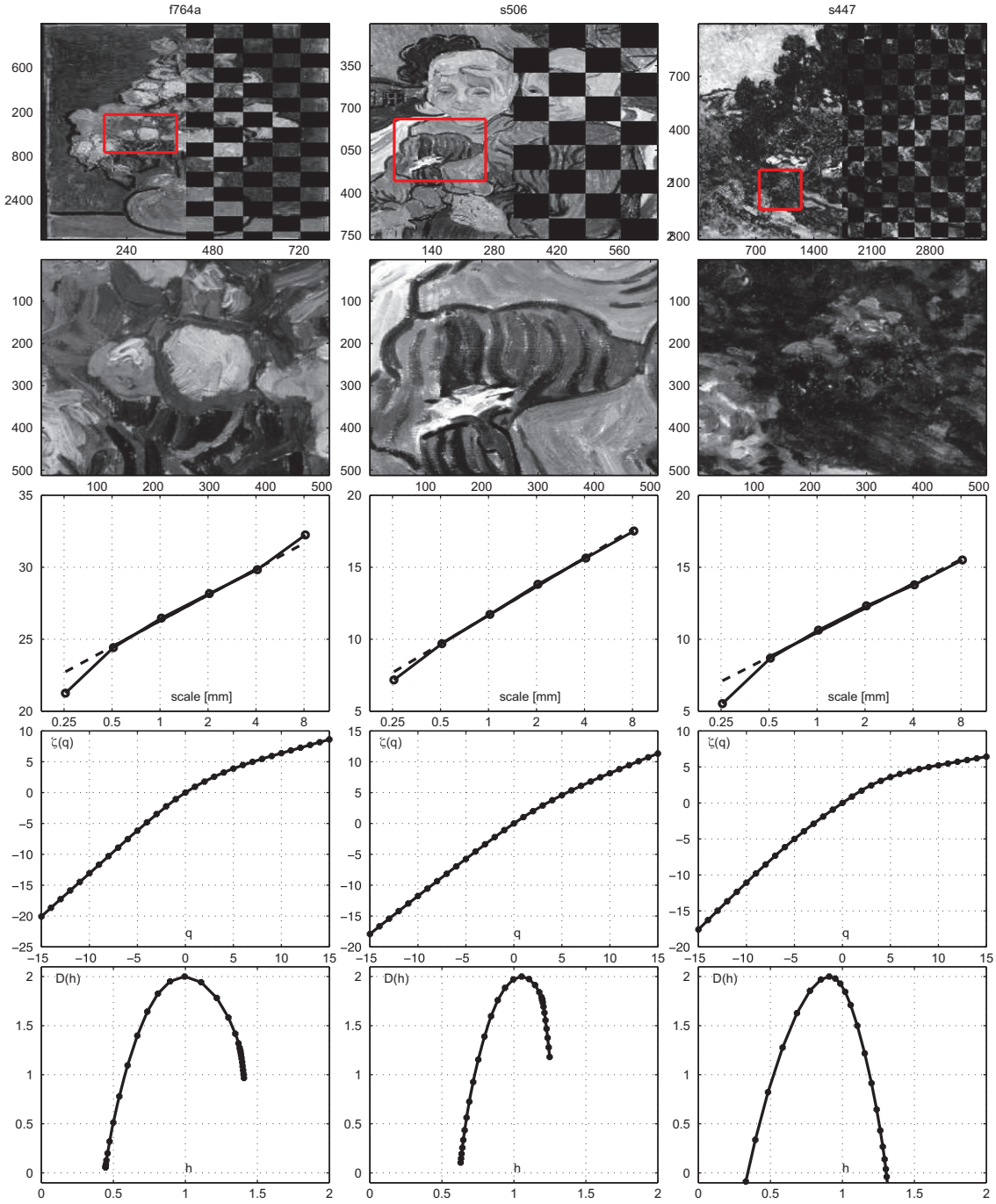

Fig. 13. Authenticity challenge: Van Gogh's vs. non-Van Gogh's paintings. Multifractal spectra computed on patches extracted from the Red Channel of Van Gogh's (left) and non-Van Gogh's (right) Paintings compared to the painting under test (middle).

consist of collections of different textures and/or of different objects and subjects. Instead, a meaningful analysis requires the careful selection of patches consisting of homogeneous textures. This is where interventions of art experts could prove useful: they may be able to identify specific patches which are of particular interest with respect to the techniques used, the status of the colors, the specificity of a particular part of a painting, etc.

At the painting level, it is worth mentioning that the range of scales where fractal properties were found to hold (from $0.5 \times 0.5\ \mathrm{mm}^2$ to $5 \times 5\ \mathrm{mm}^2$) are identical for the Princeton experiment and for Van Gogh's paintings (despite being scanned at different resolutions). This result has been obtained independently for the two data sets by different authors of this work. Again, interpretation of why this range of scales carries fractal properties

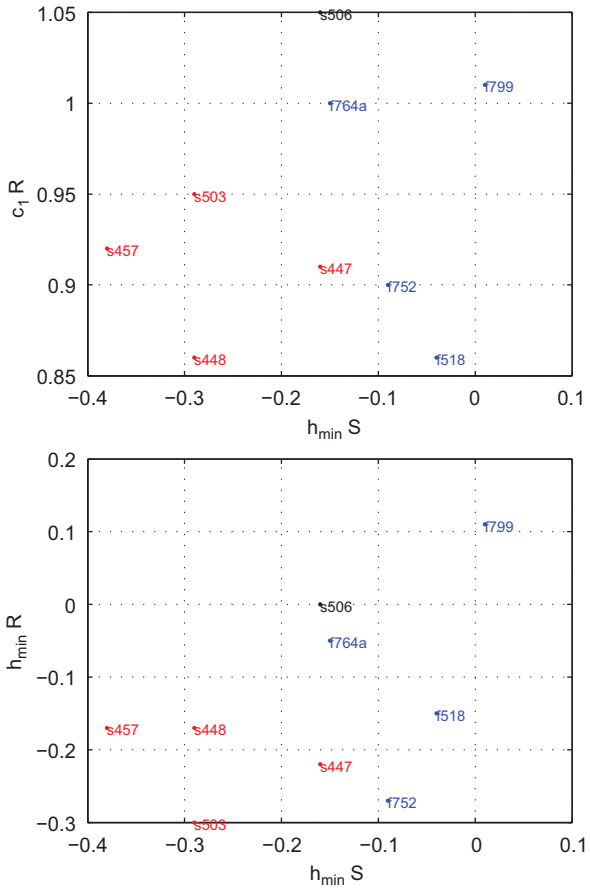

Fig. 14. Authenticity challenge: Van Gogh's vs. non-Van Gogh's paintings. Plots of h_m computed from the Saturation Channel vs. c_1 (top) and h_m (bottom) from the Red Channel suggest that painting *s*506 is closer to the Van Gogh cluster (blue) than to the Non-Van Gogh cluster (red). (For interpretation of the references to color in this figure legend, the reader is referred to the web version of this article.)

in painting would benefit significantly from close interaction with art experts. Also, given a specific interest or question, art experts could contribute considerably to the type of analysis proposed here by suggesting which patch of a painting should be analyzed in priority.

The results obtained in this contribution encouragingly demonstrating that multifractal analysis enables the measurement of features which fruitfully characterize painting texture. These first results could be further complemented and improved, by incorporating a larger number and different types of attribute estimates in the analysis. In this perspective, measures of anisotropy are currently being investigated.

Again, the analysis tools put forward here in no way intend to replace the art historian of expert in an attribution decision or else. Instead, it aims at providing them with a set of attributes computed in an automated, controlled and reproducible manner that will contribute as one of the pieces in the puzzle leading to an attribution decision. Hopefully, results such as those obtained here will help to promote existing close interactions between image processing researchers and art experts and encourage new ones. Such exchanges could enable the creation of further data sets for which both art expertise and technical issues (such as scanning resolution and techniques) are well documented, as well as the constitution of real interdisciplinary teams within which art experts would propose questions for which image processing could help to formulate answers.

Acknowledgments

The authors gratefully acknowledge the leaders of the *Image Processing for Art Investigation* project for having warmly welcome them in this research program. R. Johnson, D. Rockmore and I. Daubechies are specifically acknowledged. The Van Gogh and Kröller-Müller Museums (The Netherlands) have made this work possible by making numerous paintings available within the framework of the *Image Processing for Art Investigation* project. The Princeton research team (notably S. Hughes and I. Daubechies) is acknowledged for providing us access to the Princeton experiment data and for providing us with crucial information related to the conditions under which the experiment was conducted. S. Hughes and E. Postma are gratefully acknowledged for their kind help in Data handling. S. Hughes and M. Martens are also gratefully acknowledged for their valuable comments on the results obtained in this work and further potential developments. J. Coddington (Chief Conservator at the MoMA) and E. Hendriks (Chief Conservator at the Van Gogh museum) significantly helped improve this work with valuable discussions, notably on space scales. They are gratefully acknowledged.

This work has been partially supported by the Del Duca Foundation, Institut de France, Young Research Team Award 2007.

References

[1] P. Abry, S. Jaffard, H. Wendt, Irregularities and scaling in signal and image processing: multifractal analysis, in: M. Frame (Ed.), Benoit Mandelbrot: A Life in Many Dimensions, Yale University, USA, to appear.
[2] A. Arneodo, N. Decoster, S.G. Roux, A wavelet-based method for multifractal image analysis. I. Methodology and test applications on isotropic and anisotropic random rough surfaces, European Physical Journal B 15 (3) (2000) 567–600.
[3] B. Castaing, Y. Gagne, M. Marchand, Log-similarity for turbulent flows, Physica D 68 (3–4) (1993) 387–400.
[4] P. Chainais, Infinitely divisible cascades to model the statistics of natural images, IEEE Transactions on Pattern Analysis and Machine Intelligence 29 (12) (2007).
[5] I. Daubechies, Ten Lectures on Wavelets, SIAM, New York, 1992.
[6] J. Delour, J.F. Muzy, A. Arneodo, Intermittency of 1d velocity spatial profiles in turbulence: a magnitude cumulant analysis, European Physical Journal B 23 (2) (2001) 243–248.
[7] E. Hendriks, S. Hughes, Van Gogh's brushstrokes: Marks of authenticity? Proceedings of Art, Conservation, and Authenticities: Material, Concept, Context, 2009.
[8] Th. Hurtut, Y. Gousseau, Ch. Farida, F. Schmitt, Pictorial analysis of line-drawings, in: M. Frame (Ed.), Computational Aesthetics in Graphics (CAe'08), Eurographics, 2008, pp. 123–130.
[9] S. Jafarpour, G. Polatkan, E. Brevdo, S. Hughes, A. Brasoveanu, I. Daubechies, Stylistic analysis of paintings using wavelets and machine learning, in: Proceedings of the European Signal Processing Conference (EUSIPCO), 2009.
[10] S. Jaffard, Wavelet techniques in multifractal analysis, in: M. Lapidus, M. van Frankenhuijsen (Eds.), Fractal Geometry and Applications: A Jubilee of Benoît Mandelbrot, Proceedings of

Symposia in Pure Mathematics, American Mathematical Society, vol. 72(2), 2004, pp. 91–152.
[11] S. Jaffard, B. Lashermes, P. Abry, Wavelet leaders in multifractal analysis, in: T. Qian, M.I. Vai, X. Yuesheng (Eds.), Wavelet Analysis and Applications, Birkhäuser Verlag, Basel, Switzerland, 2006, pp. 219–264.
[12] C.R. Johnson Jr., E. Hendriks, I.J. Berezhnoy, E. Brevdo, S.M. Hughes, I. Daubechies, J. Li, E. Postma, J.Z. Wang, Processing for artist identification: computerized analysis of Vincent Van Gogh's painting brushstrokes, IEEE Signal Processing Magazine (Special Section Signal Processing in Visual Cultural Heritage) 25 (2008) 37–48.
[13] J. Li, L. Yao, E. Hendriks, J.Z. Wang, Rhythmic brushstrokes distinguish Van Gogh from his contemporaries: findings via automated brushstroke extraction, IEEE Transactions on Pattern Analysis and Machine Intelligence, 99(preprints) (2011).
[14] S. Mallat, A Wavelet Tour of Signal Processing: The Sparse Way, Academic Press, Burlington, MA, 2009.
[15] G. Polatkan, S. Jafarpour, E. Brevdo, S. Hughes, A. Brasoveanu, I. Daubechies, Detection of forgery in paintings using supervised learning, in: Proceedings of the IEEE International Conference on Image Processing (ICIP), 2005.
[16] R.H. Riedi. Multifractal processes, in: P. Doukhan, G. Oppenheim, M.S. Taqqu (Eds.), Theory and Applications of Long Range Dependence, Birkhäuser, 2003, pp. 625–717.
[17] S. Robinson, Can mathematical tools illuminate artistic style? SIAM News, 〈http://www.siam.org/news/news.php?id=34〉, 2005.
[18] D. Rockmore, J. Coddington, J. Elton, Y. Wang, Multifractal Analysis for Jackson Pollock, SPIE, 2008, pp. 6810–6813.
[19] D. Rockmore, S. Lyu, H. Farid, A digital technique for art authentication, Proceedings of the National Academy of Sciences (2004) 17006–17010.
[20] M. Sipics, The Van Gogh project: art meets mathematics in ongoing international study, SIAM News, 〈http://www.siam.org/news/news.php?id=1568〉, 2009.
[21] D.G. Stork, J. Coddington (Eds.), Computer Image Analysis in the Study of Art, Proceedings of SPIE, vol. 6810, 2008.
[22] D.G. Stork, J. Coddington, A. Bentkowska-Kafel (Eds.), Computer Vision and Image Analysis of Art II, Proceedings of SPIE, vol. 7869, 2011.
[23] M.M. Van Dantzig, Vincent? A New Method of Identifying the Artist and his Work and of Unmasking the Forger and his Products, Keesing, Amsterdam, 1953.
[24] L.J.P. van der Maaten, E.O. Postma, Texton-based analysis of paintings, Proceedings of SPIE, vol. 7798, 2010.
[25] D. Veitch, P. Abry, M.S. Taqqu, On the automatic selection of the onset of scaling, Fractals 4 (11) (2003) 377–390.
[26] D. Veitch, M.S. Taqqu, P. Abry, Meaningful MRA initialization for discrete time series, Signal Processing 80 (2000) 1971–1983.
[27] H. Wendt, Contributions of Wavelet Leaders and Bootstrap to Multifractal Analysis: Images, Estimation Performance, Dependence Structure and Vanishing Moments. Confidence Intervals and Hypothesis Tests, Ph.D. Thesis, ENS Lyon, 2008.
[28] H. Wendt, P. Abry, S. Jaffard, Bootstrap for empirical multifractal analysis, IEEE Signal Processing Magazine 24 (4) (2007) 38–48.
[29] H. Wendt, P. Abry, S. Jaffard, H. Ji, Z. Shen, Wavelet leader multifractal analysis for texture classification, in: Proceedings of the IEEE International Conference on Image Processing (ICIP), Cairo, Egypt, 2009.
[30] H. Wendt, S.G. Roux, P. Abry, S. Jaffard, Wavelet leaders and bootstrap for multifractal analysis of images, Signal Processing 89 (2009) 1100–1114.